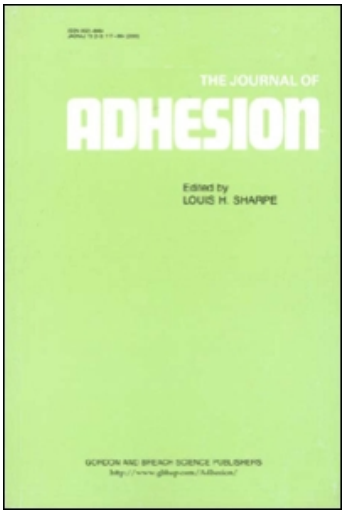

The Journal of Adhesion
Publication details, including instructions for authors and subscription information:
http://www.informaworld.com/smpp/title~content=t713453635

Root Rotation and Plastic Work Effects in the Peel Test

J. G. Williams[a]
[a] Department of Mechanical Engineering, Imperial College of Science, Technology & Medicine, London, UK

To cite this Article Williams, J. G.(1993) 'Root Rotation and Plastic Work Effects in the Peel Test', The Journal of Adhesion, 41: 1, 225 — 239
To link to this Article: DOI: 10.1080/00218469308026564
URL: http://dx.doi.org/10.1080/00218469308026564

J. Adhesion, 1993, Vol. 41, pp. 225–239
Reprints available directly from the publisher
Photocopying permitted by license only

Printed in the United States of America.

Root Rotation and Plastic Work Effects in the Peel Test*

J. G. WILLIAMS

Department of Mechanical Engineering, Imperial College of Science, Technology & Medicine, Exhibition Road, London SW7 2BX, UK

(Received September 30, 1992; in final form March 8, 1993)

A review of the analysis to determine the global energy release rate in the peel test is given. The local bending at the root is then analysed using large displacement elastic beam theory and the role of the beam root rotation in partitioning the energy between bending and direct transmission is demonstrated. The analysis is further refined using an elastic-plastic solution incorporating a model for predicting the root rotation. The resulting solution appears to predict observed variations in peel energy with thickness and angle.

KEY WORDS large displacement elastic analysis; elastic-plastic analysis; model for predicting root rotation; global energy analysis; energy loss on bending.

1. INTRODUCTION

Peel testing has a long history [*e.g.* Refs. 1–6] and has been subjected to a wide range of analyses. It arose originally from that school of fracture mechanics derived directly from the work of Griffith and used to study the fracture of rubber.[7,8] The large, non-linear elastic deformations led to a need for testing configurations which could be calibrated directly and such a test was the "trouser-leg" tear test shown in Figure 1. Tearing was observed to be at constant force, F, and the displacement of that force was seen to be twice the tear growth so that the energy per unit area, G, was thus given by:

$$G = \frac{2F}{h} \tag{1}$$

Any elastic deformations were usually small for the loads used and gave insignificant errors. It was recognised that the local conditions at the tear might be rather complex but concluded that equation (1) gave a fair measure of the energy to cause fracture. Since rubber was used, no problems of dissipating energy in the arms of the specimens were considered.

*One of a Collection of papers honoring A. J. Kinloch, the recipient in February 1992 of *The Adhesion Society Award for Excellence in Adhesion Science, Sponsored by 3M.*

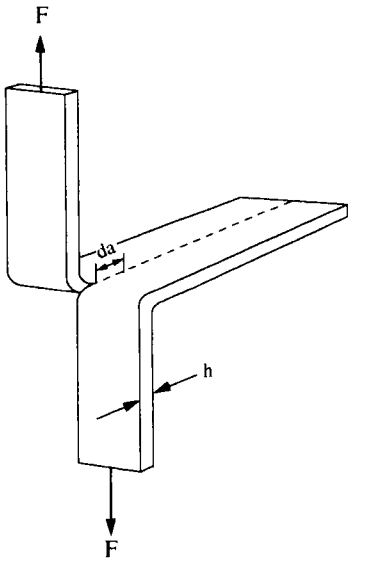

FIGURE 1 The "trouser leg" tear test.

The 90° peel test shown in Figure 2 is a direct derivative of the above and, for a width b, we have external work done for a debonding of length da of

$$P.da$$

giving a new area of b.da and hence

$$G = \frac{P}{b} \tag{2}$$

Again, any local effects or elastic deformations are ignored and the analysis has been very successful for evaluating the adherence of flexible elastic tapes.

Possible problems were identified when highly extensible rubbery strips were used[9] and refinements were introduced into the analysis to correct for the large

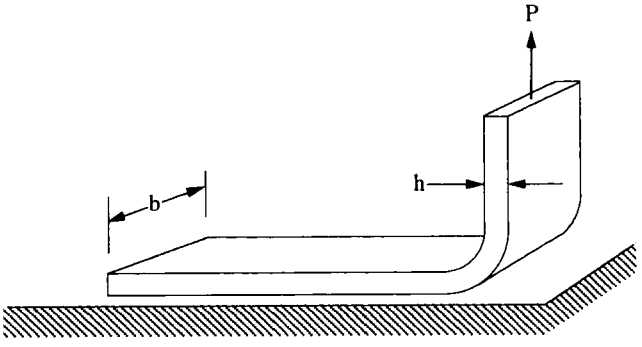

FIGURE 2 The 90° peel test.

elastic deformations. However, when the method was used for other polymers, there was some doubt over the problems of energy dissipation in the arms. Such concerns came about when laminated plastic packaging materials were analysed for inter layer adhesion. Similarly, the electronics industry has increasingly used laminates of plastics and metals and again used peel tests to evaluate adhesion. Here, the obvious plastic deformation of the metals have raised doubts about the analyses. These doubts have prompted studies using different peeling angles and different thicknesses of both adhesive and adherend. The results, and attempts to rationalise them, have been far from clear. This paper revisits some of the analyses used and some of the experimental results in an attempt to throw light on the problem.

2. THE GLOBAL ANALYSIS

The energy release rate for any system may be calculated from[10]

$$G = \frac{dU_{ext}}{b\,da} - \frac{dU_s}{b\,da} - \frac{dU_d}{b\,da} - \frac{dU_k}{b\,da} \tag{3}$$

where U_{ext} is the external work done,
U_s is the strain energy,
U_d is the dissipated energy,
U_k is the kinetic energy,
and b.da is the fracture area created by a crack growth of da for a uniform width assumed here.

If we consider the general case of the peel test with a constant load at an angle, θ, as shown in Figure 3, it is of interest to take the limiting case of a flexible but inextensible strip. For a strip originally in the horizontal position, the displacement of the load point A has the components

$$u = a(1 - \cos\theta) \quad \text{and} \quad v = a\sin\theta$$

and the movement of the load point in the direction of the load is $a(1-\cos\theta)$. Thus, for a delamination distance of da, the load point moves $da(1-\cos\theta)$ and

$$\frac{dU_{ext}}{b\,da} = \frac{P}{b}(1 - \cos\theta) \tag{4}$$

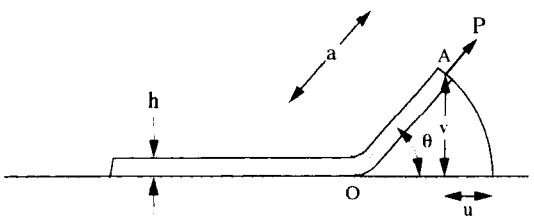

FIGURE 3 The general peel test.

For the material properties assumed here, $U_s = U_d = 0$ and for the static case $U_k = 0$ also, and hence

$$G = \frac{P}{b}(1 - \cos\theta) \tag{5}$$

the well-known result. A dynamic solution may be derived easily here, since

$$\frac{dU_k}{b\,da} = \frac{1}{2}\rho h(\dot{u}^2 + \dot{v}^2) = \rho h\dot{a}^2(1 - \cos\theta)$$

and

$$G = \left(\frac{P}{b} - \rho h\dot{a}^2\right)(1 - \cos\theta) \tag{6}$$

If G_c is the fracture resistance, then the critical value of P is

$$P_c = \frac{G_c b}{1 - \cos\theta}$$

and, for $P > P_c$, the delamination speed for $G = G_c$ is

$$\dot{a}^2 = \frac{P - P_c}{\rho b h} \tag{7}$$

It is thus possible to account for the dynamic behaviour of such a system including unstable crack growth [*e.g.* Ref. 11].

If the strip is assumed to be linearly elastic, then the load P induces a strain given by

$$e = \left(\frac{P}{bh}\right)\frac{1}{E} \tag{8}$$

where E is Young's modulus. The displacement of the load point is now

$$a(1 - \cos\theta + e)$$

and the change in strain energy is

$$\frac{dU_s}{b\,da} = \frac{Ehe^2}{2}$$

and hence

$$G = \frac{P}{b}(1 - \cos\theta + e) - \frac{Ehe^2}{2} = Eh\left[e(1 - \cos\theta) + \frac{e^2}{2}\right] \tag{9}$$

In most cases, $e^2/2 \ll e(1 - \cos\theta)$, though for highly elastic systems it is necessary to make corrections.[9] It should be noted here that extra external work is done by stretching the strip by a e and that, for this sustained load case, the change in U_s is the energy put into the increase in length da. For the same constant load condition, we may now consider any stress-strain relationship which may include dissipation.[11] If there is a strain, e, in the strip, then

$$\frac{dU_{ext}}{b\,da} = \frac{P}{b}(1 - \cos\theta + e)$$

as before, and

$$\frac{d(U_s+U_d)}{b\,da}=h\int_0^e \sigma\,de$$

with

$$\sigma=\frac{P}{b\,h}$$

and hence

$$G=h\left[\sigma(1-\cos\theta)+\sigma e-\int_0^e \sigma\,de\right]=h\left[\sigma(1-\cos\theta)+\int_0^\sigma e\,d\sigma\right] \tag{10}$$

Although there may be energy dissipated in the strip, G is still increased because the external work *via* the constant load provides the necessary energy. For an elastic-perfectly plastic material with a yield stress of σ_y, we have

$$G=h\left[\sigma_y(1-\cos\theta)+\frac{\sigma_y^2}{2E}\right]=Eh\left[e_y(1-\cos\theta)+\frac{e_y^2}{2}\right] \tag{11}$$

i.e. the elastic result limited by the yield strain $e_y=\sigma_y/E$. The actual strain may be much greater than e_y but G cannot be greater than that given in equation (11).

It should also be noted that the second term in equation (10) becomes predominant for $\theta=0$, but this case is not really a peel test but rather an axially loaded strip.[11] For all significant values of θ, which constitute a true peel test, the first term arising from external work is predominant.

3. LOCAL MOMENT ELASTIC SOLUTIONS

Explanations for some very complex behaviour that has been observed in peel tests have been sought in the analysis of the region near the base of the strip where it is stuck down [*e.g.* see Ref. 6]. If it is assumed that the slope at the contact point is zero, then the geometry is as shown in Figure 4. If we assume that all the energy release is transmitted *via* bending, then we may compute the moment at the base, M_o, by equating the local G to that applied; *i.e.*

$$G=\frac{P}{b}(1-\cos\theta)=\frac{6M_o^2}{Eb^2h^3}$$

i.e.

$$M_o^2=\frac{Ebh^3}{6}P(1-\cos\theta) \tag{12}$$

The maximum bending strain is given by

$$e_B=\frac{6M_o}{bh^2E}=\sqrt{6e(1-\cos\theta)} \tag{13}$$

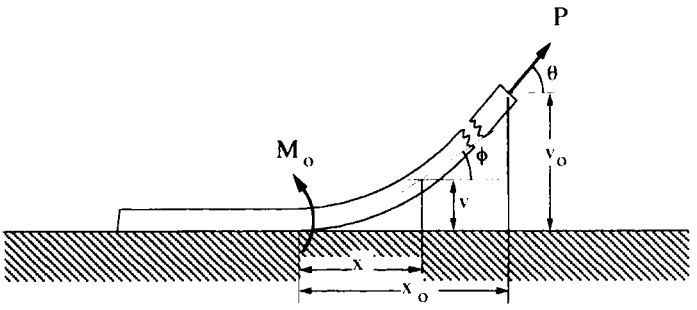

FIGURE 4 Local moments.

so that, for example, an axial strain of 0.01 in a 90° peel test gives a bending strain of 0.24, *i.e.* a substantial magnification. A limit on the elastic behaviour may also be computed[12,13] for the condition $e_B = e_y$, the yield strain, which puts a severe constraint on e. For example, for $e_y = 0.06$, a typical value for polymers, $e = 6 \times 10^{-4}$ and the maximum available G is given by $G = Ehe$, and for $E = 3$ GPa and $h = 100$ μm we have $G = 180$ J/m^2. Typical adhesion tests give G values of several hundreds of J/m^2 and are thus operating in the plastic region locally.

It is instructive, at this stage, to consider the large displacement beam solution[14] for the root region and this is conveniently couched in terms of the slope, φ, so that

$$\sin\phi = \frac{dv}{ds}, \quad \cos\phi = \frac{dx}{ds} \quad \text{and} \quad \frac{d\phi}{ds} = \frac{1}{R} \tag{14}$$

where R is the radius of curvature, and s is the arc length of the beam. The moment at any point is

$$M = P\,[(x_o - x)\sin\theta - (v_o - v)\cos\theta] \tag{15}$$

where x_o and v_o are the coordinates of the load point, as shown in Figure 4. Since the deformation is elastic and predominantly bending, we have

$$\frac{1}{R} = \frac{12M}{Ebh^3} \tag{16}$$

Differentiating equations (15) and (16) with respect to φ and noting the relationships in equations (14), we have

$$\frac{1}{R^3}\frac{dR}{d\phi} = \frac{12P}{Ebh^3}\sin(\theta - \phi) \tag{17}$$

It is now important to consider what happens when the slope at the contact point is not zero but takes a value θ_o. We may integrate equation (17) between the base with $R = R_o$ and $\phi = \theta_o$ and the load region for which $R = \infty$ and $\phi = \theta$. Thus,

$$\frac{1}{2R_o^2} = \frac{12P}{Ebh^3}[1 - \cos(\theta - \theta_o)] = \frac{1}{2}\left[\frac{12M_o}{Ebh^3}\right]^2 \tag{18}$$

i.e.

$$M_o^2 = \frac{Ebh^3}{6}.\, P\,[1-\cos(\theta-\theta_o)] \tag{19}$$

Note that if $\theta_o = 0$, then we retrieve equation (12) but, if not, then only a proportion of the energy is transmitted *via* bending, the rest going directly to the peeling process. The directly transmitted value of G, G_o, is thus

$$G_o = \frac{P}{b}(1-\cos\theta) - \frac{6M_o^2}{Eb^2h^3} = \frac{P}{b}[\cos(\theta-\theta_o) - \cos\theta] \tag{20}$$

and if $\theta_o = 0$, $G_o = 0$, as expected. Note that if $\theta = \theta_o$, then all the energy is directly transmitted and, of course, there is no bending.

It is possible to estimate θ_o since the section of the strip beyond the contact point acts as a beam on an elastic foundation formed by half the strip thickness.[15,16,17] This method has been used to correct composite beam data [*e.g.* see Ref. 18] and good accuracy can be obtained by assuming that the beam is actually 2/3 h longer, as shown in Figure 5. At the root,

$$\frac{1}{R_o} = \frac{d\phi}{ds} = \frac{3\theta_o}{2h}, \quad i.e. \quad \theta_o = \frac{2h}{3R_o} \tag{21}$$

and an expression for θ_o can be deduced using equation (18), *i.e.*

$$\theta_o^2 = \left(\frac{32}{3}\right) e\,[1-\cos(\theta-\theta_o)] \tag{22}$$

and equation (20) can be written as a ratio of G_o to G, *i.e.*

$$\frac{G_o}{G} = \frac{\cos(\theta-\theta_o) - \cos\theta}{1-\cos\theta} \tag{23}$$

Table I gives computed values for $\theta = 90°$ showing how θ_o varies with the tensile strain, e, and thus G, since

$$e = \frac{P}{Ebh} = \frac{G}{Eh} \quad \text{for } \theta = 90°$$

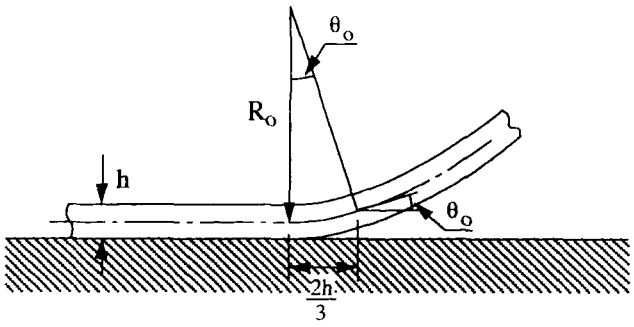

FIGURE 5 Root rotation in the peel test.

TABLE I
$\theta = 90°$

$\theta_o°$	10	20	30	40	50
e	3.5×10^{-3}	0.0175	0.052	0.128	0.306
G_o/G	0.174	0.342	0.500	0.643	0.766

In the elastic case, of course, no energy is lost so the delivered G is that applied. An approximation to energy dissipation occurring in bending is simply to assume that only G_o is available and this is a useful model of the highly work hardening case. True G values, *i.e.* G_o, can be found from determining e and hence G_o/G. For the numbers used earlier in this section, for example $E = 3$ GPa, $h = 100$ μm, and if we assume a strain of 3.5×10^{-3} ($\theta_o = 10°$), then $G = 1050$ J/m^2 and $G_o = 183$ J/m^2.

4. LOCAL MOMENT ELASTIC-PLASTIC SOLUTIONS

A better model of the energy dissipation process in bending the strip may be found by considering the behaviour of an elastic-perfectly plastic material for which

$$\sigma = Ee \quad , \quad e < e_Y$$

and

$$\sigma = \sigma_y = Ee_y \quad , \quad e > e_Y$$

If a beam is bent such that in the outer fibres $e > e_Y$, then the stress distribution is as shown in Figure 6 and the moment is given by

$$M = M_p\left(1 - \frac{1}{3}\frac{c^2}{h^2}\right) \tag{24}$$

where c is the depth of the elastic core region and $M_p = (b\, h^3\, Ee_y)/4$, the fully plastic maximum moment when $c = 0$. The radius of curvature can be defined in terms of the elastic core since

$$R = \frac{c}{2e_y}$$

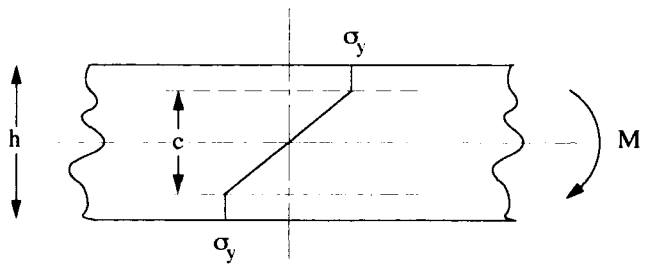

FIGURE 6 Elastic-plastic stress distribution.

and we may define R at first yield as

$$R_1 = \frac{h}{2e_y}$$

and hence

$$\frac{R}{R_1} = \frac{c}{h} = x \tag{25}$$

where x is the elastic core or radius ratio. The curvature moment relationship for the elastic-plastic case is thus:

$$\frac{R_1}{R} = \frac{1}{x} = \frac{1}{\sqrt{3(1 - M/M_p)}} \tag{26}$$

and the elastic form, equation (16), can be rewritten as

$$\frac{R_1}{R} = \frac{1}{x} = \frac{3}{2}\frac{M}{M_p} \tag{27}$$

These relationships are shown in Figure 7 with equation (27) pertaining for $1/x<1$ and equation (26) for $1/x>1$. The work done per unit length of beam, W, is found from the area under this curve, 0AA′, and hence

$$\left.\begin{aligned} &\frac{1}{x}<1 \quad , \quad W = \hat{G}\int_0^{1/x}\left(\frac{M}{M_p}\right) d\left(\frac{1}{x}\right) = \hat{G}\left(\frac{1}{3x^2}\right) \\ &\text{and} \\ &\frac{1}{x}>1 \quad , \quad W = \frac{\hat{G}}{3} + \hat{G}\int_1^{1/x}\left(\frac{M}{M_p}\right) d\left(\frac{1}{x}\right) = \hat{G}\left(\frac{1}{x} + \frac{x}{3} - 1\right) \end{aligned}\right\} \tag{28}$$

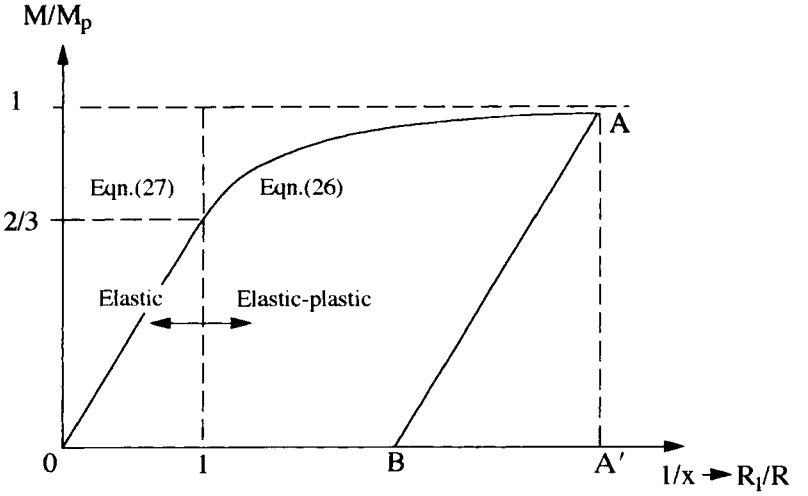

FIGURE 7 Moment curvature relationship for an elastic-perfectly plastic beam.

where

$$\hat{G} = \frac{Ehe_y^2}{2}$$

the maximum elastic energy per unit length which can be stored in the beam. The energy which can be recovered on unloading the beam is the area BAA′ in Figure 7 and is

$$\left.\begin{aligned} &\frac{1}{x}<1 \quad , \quad W = \hat{G}\left(\frac{1}{3x^2}\right) \\ \text{and} \\ &\frac{1}{x}>1 \quad , \quad W = \hat{G}\,\frac{3}{4}\left(1-\frac{x^2}{3}\right)^2 \end{aligned}\right\} \tag{29}$$

An elegant experiment is reported in Reference 6 which illustrates the utility of this analysis. Thin strips were bent through 180° between smooth parallel plates and the force required to draw one end continuously was measured. This is equivalent to a 180° peel test with zero G but a fixed radius of curvature given by the separation of the plates D = 2R. Assuming x<1, we have

$$\frac{P}{b} = \frac{\hat{G}}{2}\left(\frac{1}{x}+\frac{x}{3}-1\right) \tag{30}$$

The results plus this function fitted with E = 5.1 GPa and $e_y = 0.018$ are shown in Figure 8 and illustrate the general accuracy of the analysis.

In the real peel test, R is not predetermined and is governed by G and leads to rather complex behaviour. This has been analysed in a series of excellent papers by Aravas and Kim.[19,20,21] They point out that in steady-state peeling, a moment, M_o,

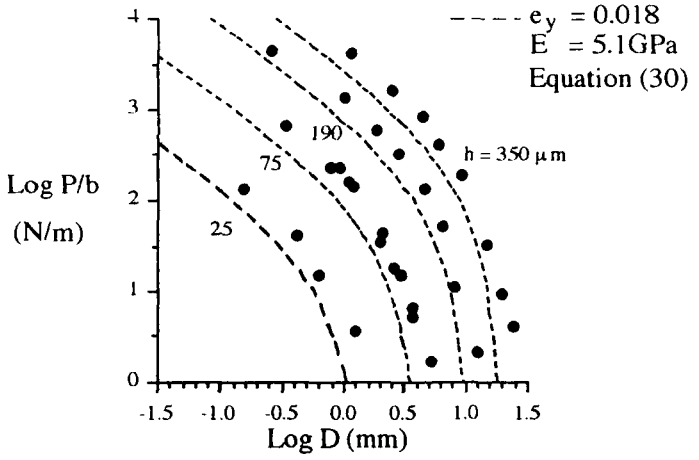

FIGURE 8 Plastic bending force as a function of diameter, D = 2R. Data from Reference 6.

is applied at the root and that the strip unloads continuously as steady-state peeling proceeds until it is straight and $R \to \infty$, *i.e.* $1/x = 0$. Thus, in the M/M_p *versus* $1/x$ diagram, the end point is always on the $1/x = 0$ axis. Two possible loading paths are shown in Figure 9(a). In (i), M_o is applied from 0 to A at the root and then unloads elastically to B. There is, thus, always a residual curvature which must be taken out by an offset of P as shown in Figure 9(b). When the load is removed, the radius will return to B′ giving a residual curl in the strip. The energy per unit length dissipated in the process is thus 0AB′B which is the second of equations (28) with the addition of the area 0B′B and subtracting the second of equations (29). The former is not available for propagation but is recovered on unloading. Thus, we have

$$W_{(i)} = \hat{G}\left(\frac{1}{3x^2} + \frac{2x}{3} - 1\right) \tag{31}$$

This behaviour will pertain until the unloading induces plastic unloading, as shown in line (ii) in Figure 9(a). The transition is at $x = 0.5$ and, for $x < 0.5$, the area 0ACD must be found and is[19]

$$W_{(ii)} = \hat{G}\left(\frac{2}{x} + \frac{10x}{3} - 5\right) \tag{32}$$

Note that for $x \ll 1$ the dominant term is $2/x$, the area of the rectangle $2 \times 1/x$ in Figure 9. Also note that, for this condition, the residual radius of curvature tends to $R_1 = h/2e_y$.

The deformation of the strip during the unloading phase in case (i) is elastic and so equation (18) still applies and may be rewritten in terms of x as

$$\frac{1}{3x^2} = \frac{G}{\hat{G}}\left[\frac{1 - \cos(\theta - \theta_o)}{1 - \cos\theta}\right] \tag{33}$$

For case (ii), part of the unloading is elastic-plastic and involves using equation (26); the result is[19]:

$$\frac{2}{x} + \frac{8x}{3} - 4 = \frac{G}{\hat{G}}\left[\frac{1 - \cos(\theta - \theta_o)}{1 - \cos\theta}\right] \tag{34}$$

The G value delivered to the interface is now

$$G_o = \frac{P}{b}(1 - \cos\theta) - W_{(i),(ii)}$$

and we have the two cases

$$\left.\begin{aligned} &\text{(i)} \quad x > \tfrac{1}{2} \quad , \quad \frac{1}{3x^2} = \frac{G}{\hat{G}}\left[\frac{1 - \cos(\theta - \theta_o)}{1 - \cos\theta}\right] \quad , \quad \frac{G_o}{\hat{G}} = \frac{G}{\hat{G}} - \left(\frac{1}{3x^2} + \frac{2x}{3} - 1\right) \\ &\text{and} \\ &\text{(ii)} \quad x < \tfrac{1}{2} \quad , \quad \frac{2}{x} + \frac{8x}{3} - 4 = \frac{G}{\hat{G}}\left[\frac{1 - \cos(\theta - \theta_o)}{1 - \cos\theta}\right] \quad , \quad \frac{G_o}{\hat{G}} = \frac{G}{\hat{G}} - \left(\frac{2}{x} + \frac{10x}{3} - 5\right) \end{aligned}\right\} \tag{35}$$

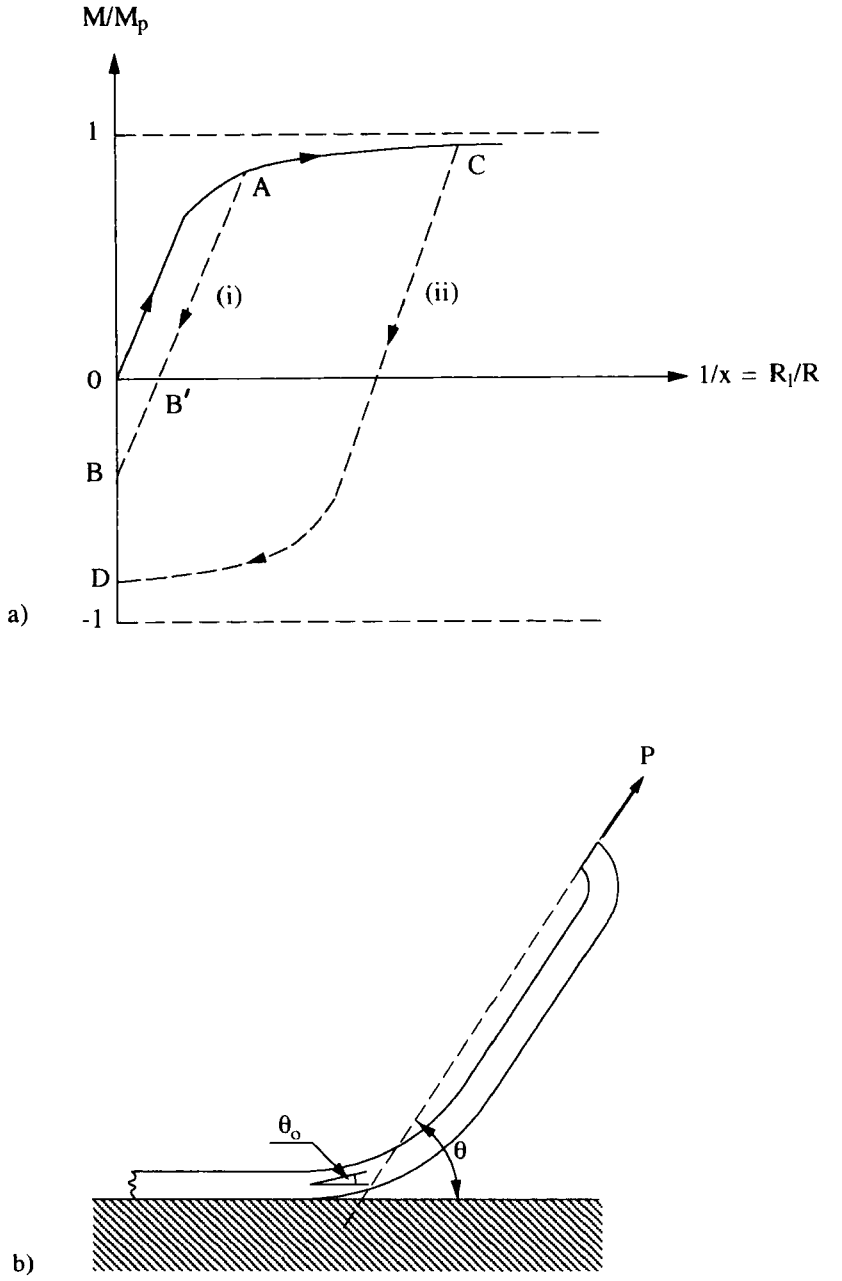

FIGURE 9 Unloading in peeling: a) Unloading paths in peeling; b) Reverse bending in peel test.

As in the elastic case, we can find θ_o *via* equation (21)

$$\theta_o = \frac{2}{3}\frac{h}{R_o} = \frac{4}{3}\frac{e_y}{x} \tag{36}$$

Equations (35) and (36) can be solved by iteration for any value of $G/\hat{G}$ to give G_o/G, but a useful result for $x \ll 1$ is

$$\frac{G_o}{G} = \frac{\cos(\theta - \theta_o) - \cos\theta}{1 - \cos\theta}$$

as in the elastic case, assuming all the bending energy is lost, and

$$\frac{3}{2e_y} \cdot \theta_o = 4 + \frac{G}{\hat{G}}\left[\frac{1 - \cos(\theta - \theta_o)}{1 - \cos\theta}\right] \tag{37}$$

replacing equation (22).

A set of data is shown in Figures 10 and 11. In Figure 10, $G_o/\hat{G}$ is shown as a function of $G/\hat{G}$ using equations (35) and (36) for $\theta = 90°$, 135° and 180°. Also shown is the elastic solution given in Table I in which e is converted to $G/\hat{G}$ *via*

$$\frac{G}{\hat{G}} = \frac{2e}{e_y^2}$$

There is a very similar trend which indicates that the dominant effect is the almost total loss of energy in bending. Figure 11 shows the same data replotted as G/G_o *versus* G/G_o which models the effect of varying thickness for a constant G_o *via* G/G_o and measuring the resultant G value. There is a marked maximum which has been discussed previously[6,20,22] but not predicted explicitly before. It is also clear from Figure 10 that if θ is varied for given h and G_o values, then G will increase with θ. As $\theta_o \to 8e_y/3$, $G/G_o \to 1$ so small angle peel tests, *i.e.* $\theta \approx 10°$, give true values, while at $\theta = 90°$ G is two to three times G_o and at $\theta = 180°$ it can be five to 10 times,

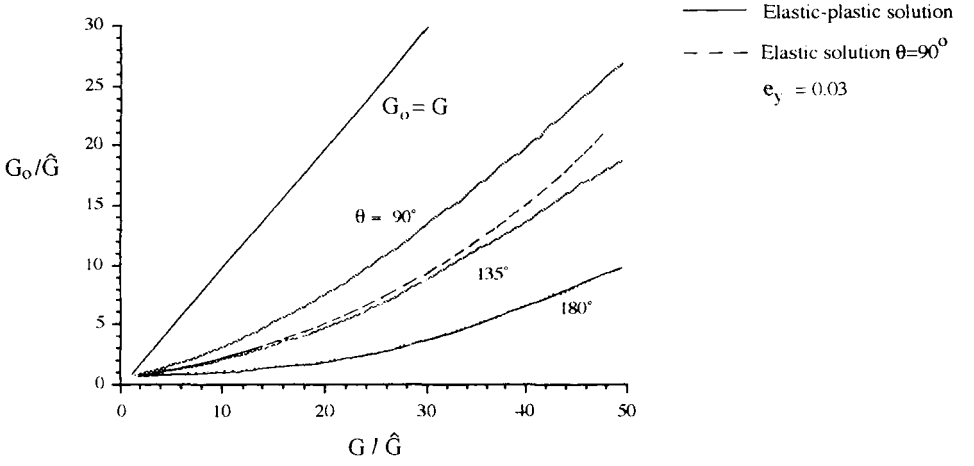

FIGURE 10 Energy release rate at interface, G_o, as a function of applied value G, $\hat{G} = \frac{Ehe_y^2}{2}$

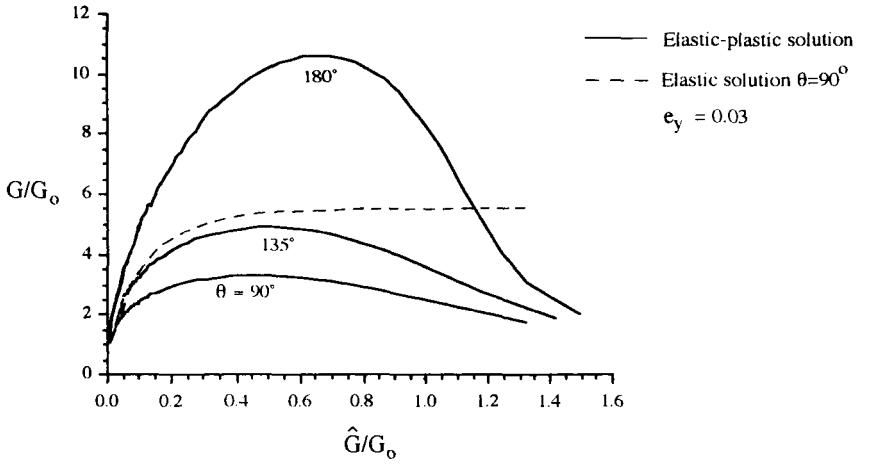

FIGURE 11 Applied G as a function of $\hat{G}$ for fixed G_o.

depending on thickness and e_y. There have been many observations that there is such an effect in tests [*e.g.* see Ref. 6] and the data reported show changes of the order given above. Rather careful analysis is required to determine if G_o is indeed constant. If not, there may be a mixed-mode fracture effect but the analysis does indicate variations of the correct order.

5. CONCLUSION

The large displacement elastic analysis demonstrates the importance of the root rotation in determining the proportion of the applied energy which goes into bending and that which goes directly to the interface. The elastic-plastic analysis allows the dissipation to be more accurately computed but the crucial step in this analysis is the relationship between θ_o and R_o. That used assumes no adhesive thickness so that all the local deformation comes from the strip itself *via* the half thickness. The model may be extended to include the adhesive thickness, h_a, and modulus, E_a, *via*

$$\theta_o = \frac{2h}{3R_o}\left(1 + \frac{2h_a}{h}\cdot\frac{E}{E_a}\right)$$

For anisotropic materials, the factor of 2/3 is increased.[17] The utility of this has yet to be explored.

It seems likely that the relationships given here will describe most of the experimental observations.

References

1. G. J. Spies, *J. Aircraft Eng.* **25,** 64–70 (1953).
2. J. Bikerman, *J. App. Phys.* **28,** 1484–85 (1957).

3. K. Kendall, *J. Phys. D.* **4,** 1186–1195 (1971).
4. K. Kendall, *J. Phys. D.* **8,** 1449–1452 (1975).
5. K. Kendall, *J. Adhesion* **5,** 105–117 (1973).
6. A. N. Gent and G. R. Hamed, *J. Appl. Polym. Sci.* **21,** 2817–2831 (1977).
7. R. S. Rivlin and A. G. Thomas, *J. Polym. Sci.* **10,** 291–318 (1953).
8. A. G. Thomas, *J. Polym. Sci.* **31,** 467–480 (1958).
9. A. N. Gent and C. W. Liu, *J. Adhesion* **30,** 1–11 (1989).
10. J. G. Williams, *Fracture Mechanics of Polymers* (Ellis Horwood Limited, London, 1984).
11. J. G. Williams, *J. Strain Analysis,* in press (1993).
12. M. D. Thouless and H. M. Jensen, *J. Adhesion* **38,** 185–197 (1992).
13. A. N. Gent and S. Y. Kaang, *J. Adhesion* **24,** 173–181 (1987).
14. J. G. Williams, *J. Comp. Mat.* **21**(4), 330–347 (1987).
15. M. F. Kanninen, *Int. J. Fract.* **9,** 83–92 (1973).
16. M. F. Kanninen, *Int. J. Fract.* **10,** 415–430 (1974).
17. J. G. Williams, *Comp. Sci. & Tech.* **35,** 367–376 (1989).
18. S. Hashemi, A. J. Kinloch and J. G. Williams, *Proc. R. Soc. Lond.* **A427,** 173–199 (1990).
19. N. Aravas, K.-S. Kim and M. J. Loukis, *Mat. Sci. & Eng.* **A107,** 159–168 (1989).
20. Y.-S. Kim and J. Kim, *J. Eng. Mat. & Tech.* **110,** 266–273 (1988).
21. Y.-S. Kim and N. Aravas, *Int. J. Solids Structures* **24**(4), 417–435 (1988).
22. H. R. Brown and A. C. M. Yang, *J. Adhesion Sci. & Tech.* **6**(3), 333–346 (1992).